Indian Journal of Pure & Applied Physics
Vol. 52, April 2014, pp. 255-261

Effect of doping cations Li(I)-, Ca(II)-, Ce(IV)- and V(V)- on the properties and crystalline perfection of potassium dihydrogen phosphate crystals: A comparative study

G Ramasamy[a], G Bhagavannarayanana[b] & Subbiah Meenakshisundaram[a]*

[a]Department of Chemistry, Annamalai University, Annamalainagar 608 002, India

[b]Head of Crystal Growth and Crystallography Division, National Physical Laboratory (NPL), Dr K S Krishnan Road, New Delhi 110 012, India

*E-mail: aumats2009@gmail.com

Received 10 June 2013; revised 30 September 2013; accepted 8 January 2014

The effect of doping metal ions with varied ionic charges (ranging from +1 to +5), Li(I)-, Ca(II)-, Ce(IV)- and V(V)- on the growth process and properties of potassium dihydrogen phosphate (KDP) crystals, grown by slow evaporation solution growth technique, has been investigated. Incorporation of metal ion into the KDP crystalline matrix is well confirmed by energy dispersive X-ray spectroscopy and atomic absorption spectroscopy. Interesting to observe that the incorporation is comparatively less in doping the higher valent metal. The powder XRD pattern and Fourier transform-IR analysis confirm the slight distortion in the structure of the KDP crystals as a result of metal ion doping. Slight changes in cell parameter values of doped KDP crystals are observed by single crystal XRD analysis. The high-resolution X-ray diffraction (HRXRD) studies used to evaluate the crystalline perfection reveal many interesting features on the ability of accommodating the dopants by the crystalline matrix. Surface morphological changes because of foreign metal ion incorporation are observed by scanning electron microscopy. UV-Vis spectroscopy reveals that the transparency is not affected much by the dopants and the cut-off wavelengths of all the doped specimens lie in a close range. Band-gap energies are estimated using optical transmittance data. Enhanced second harmonic generation efficiency is observed.

Keyword: Potassium dihydrogen phosphate, Nonlinear optical properties, Doping, HRXRD, Crystal, XRD

1 Introduction

KDP is widely used as the second, third and fourth harmonic generator for Nd:YAG and Nd:YLF lasers. The crystals are widely used for electro-optical applications as Q-switches for Nd:YAG, Nd:YLF, Ti:Sapphire and alexandrite lasers, as well as for acousto-optical applications[1-3]. KDP belongs to the tetragonal system with the space group[4] *I-42d*. It is well known that doping influences the machanical, electical, optical properties and surface morphology depending upon the nature of host material and the dopant. The influence of cations Fe^{3+}, Cr^{3+}, Al^{3+} (Refs 5-7), La^{3+} (Ref. 8), Pd^{2+} (Ref. 9), Au^{+} (Ref.10), Ce^{4+} (Refs 11, 12), Ti^{+} (Ref. 13) and Mn^{3+} (Ref. 14) on the growth and properties of KDP crystals has been extensively investigated. The structure of defect centres, growth rates and surface morphology of KDP crystals by the incorporation of bivalent (Ni^{2+}, Co^{2+}, Fe^{2+}, Mn^{2+}, Ba^{2+}, Ca^{2+}, Sr^{2+}) and trivant (Fe^{3+}, Mn^{3+}, Y^{3+}, La^{3+}) impurity ions has been studied[15,16]. Effect of anions on growth habit and characterization of KDP crystals has also been investigated[17,18].

Recently, the concentration effects of s-, p-, d- and f-block elements doping on the growth, crystalline perfection and properties of KDP crystals[19] have been investigated. In the present paper, the effect of metal ions with ionic charges ranging from +1 to +5 such as Li(I)-, Ca(II)-, Ce(IV)- and V(V)-doping on KDP crystals has been studied using FT-IR, AAS, SEM, EDS, DSC, UV-Vis and Kurtz powder SHG technique. Estimated crystalline perfections by means of nature of the rocking curves of HRXRD are compared.

2 Experimental Details

KDP (E. Merck) was purified by repeated recrystallization. Li(I)- in the form of lithium chloride (SDS), Ca(II)- in the form of calcium chloride (BDH), Ce(IV) in the form of ceric ammonium sulfate (BDH) and V(V)- in the form of vanadium pentoxide (BDH) are used as dopants. Saturated aqueous solutions of pure and 1 mol % metal doped KDP crystals were prepared. After filtration, it was preheated to 5°C above the saturation temperature and left for 3 h under

stirring to ensure homogeneity and then the saturated solution was tightly covered with a perforated paper. The crystallization took place within 15 days and the high quality transparent crystals were harvested from the aqueous growth medium. Best quality and highly transparent seed crystals are used in the preparation of bulk crystals. Photographs of as-grown bulk crystals are shown in Fig. 1.

The FT-IR spectra were recorded by using an AVATAR 330 FT-IR instrument by KBr pellet technique in the range 500-4000 cm^{-1}. Bruker AXS (Kappa Apex II) X-ray diffractometer was used for single crystal XRD studies. The powder X-ray diffraction was performed by using Philips Xpert Pro Triple-axis X-ray diffractometer at room temperature at a wavelength of 1.540 Å with a step size of 0.008°. The samples were examined with Cu Kα radiation in the 2θ range from 10 to 60°. The XRD data were analyzed by the Rietveld method with RIETAN-2000. The crystalline perfection of the grown single crystals was characterized by HRXRD by employing a multi-crystal X-ray diffractometer[20] developed at NPL. The well-collimated and monochromated Mo $K\alpha_1$ beam obtained from the three monochromator Si crystals set in dispersive (+,–,–) configuration has been used as the exploring X-ray beam. The specimen crystal is aligned in the (+,–,–,+) configuration. The DC was recorded by the so-called ω scan wherein the detector was kept at the same angular position $2\theta_B$ with wide opening for its slit. This arrangement is very appropriate to record the short range order scattering caused by the defects or by the scattering from local Bragg diffractions from agglomerated point defects or due to low angle and very low angle structural grain boundaries[21]. Before recording the diffraction curve to remove the non-crystallized solute atoms remained on the surface of the crystal and the possible layers which may sometimes form on the surfaces on crystals grown by solution methods[22] and also to ensure the surface planarity, the specimen was first lapped and chemically etched in a non-preferential etchant of water and acetone mixture in 1:2 volume ratio.

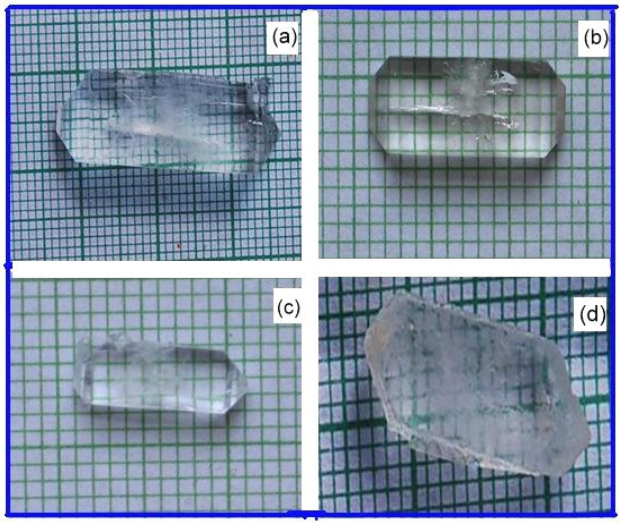

Fig. 1 — Photographs of doped KDP crystals (a) KDP:Li (b) KDP:Ca (c) KDP:Ce and (d) KDP:V

The surface morphologies were observed by using a JEOL JSM 5610 LV SEM with the resolution of 3.0 nm, an accelerating voltage 20 kV and maximum magnification 3,00,000 times. Energy dispersive X-ray spectroscopy (EDS), a chemical microanalysis technique was performed in conjunction with SEM. AAS was recorded using VARIAN Model SPECTRAA 220 spectrometer in acetone – air flame. This technique is used to quantify the concentration of the dopant present in KDP crystals using a graphite line as internal standard. UV-vis spectra were recorded using Varian Cary 5E UV-Vis-NIR spectrophotometer. DSC curves were recorded using a DSC-60 Shimadzu analyzer obtained at a heating rate of 20°C per min, between the temperature ranges 0 to 500°C in nitrogen atmosphere. The second harmonic generation (SHG) test was performed by Kurtz powder SHG method. An Nd:YAG laser with modulated radiation of 1064 nm was used as the optical source with an input radiation of 2.5 mJ/pulse and microcrystalline KDP used as a reference material.

3 Results and Discussion

FT-IR spectra of pure and 1 mol % Li(I)-, Ca(II)-, Ce(IV)- and V(V)- doped KDP crystals reveal that the doping results in shifts in some of the characteristic vibrational frequencies. The O–H bending (δ(O–H)), stretching (υ(O–H)) and $(PO_4)^{3-}$ vibration, P=O–H stretching (υ(P=O–H)) are shifted considerably and it could be due to the lattice strain developed as a result of doping. The vibrational frequencies are given in Table 1.

The effect of doping cations with varied valencies on the surface morphology of KDP crystal faces reveals the formation of structure defect centers. Fig. 2 (a) corresponding to pure KDP crystal exhibits parallel slip planes in a plate like structure. Li(I)- doped KDP, Fig. 2 (a) shows small scatter centers on the parallel plane like structure.

Ca(II)-doped specimen [Figs.2 (b)] shows more scatter centers, spots and defects in the surface. SEM pictures of Ce(IV)-and V(V)-doped crystals [Figs 2 (c and d)] reveal voids, grains and patches on the surface. It is quite clear from the micrographs that the external morphology depends on the nature of the metal.

The incorporation of foreign metal ion into the crystalline matrix was confirmed by EDS (Fig. 3). Analysis of the surface at different sites reveals that the incorporation of dopant is not very uniform throughout the surface. EDS spectra reveal only a small quantity accommodation of the doping material and it is not proportional to the amount of dopant used in the crystallization process. The metal ion incorporation is small but significant as revealed by AAS data listed in Table 2.

High percentage of transmittance in the visible region is observed for the doped specimens (Fig. 4) and hence, these are quite useful for optical device applications. The direct band gap energies can be obtained from the intercept of the resulting straight lines with the energy axis at $[F(R)\ h\nu]^2 = 0$ [where F(R) is the Kubelka-Munk function[23]] and they are listed in Table 2. The Tauc plots of the optical absorption spectrum measured at room temperature are shown in Fig. 5. Using first-principles calculations[24], the direct band gap of 4.178 eV is observed for KDP, which is significantly smaller than the experimental values[25] of 7.12 eV (~ 174 nm).

DSC analysis clearly shows that there is no physically absorbed water in the molecular structure of doped crystals. The studies reveal the purity of the

Table 1 — FT-IR frequencies of fundamental vibrations of pure and 1 mol % metal doped KDP samples (cm^{-1})

Specimen	P-O-H symmetrical stretching	P=O symmetrical stretching	P-O-H stretching (Hydrogen bonding)	O-H bending	O-P-O bending
Pure KDP	909	1660	2790, 3440	1330, 655	546
KDP : Li	909	1748	2797, 3420	1330, 650	545
KDP : Ca	911	1712	2700, 3298	1340, 664	547
KDP : Ce	920	1723	2670, 3380	1370, 630	590
KDP : V	915	1717	2715, 3390	1365, 625	548

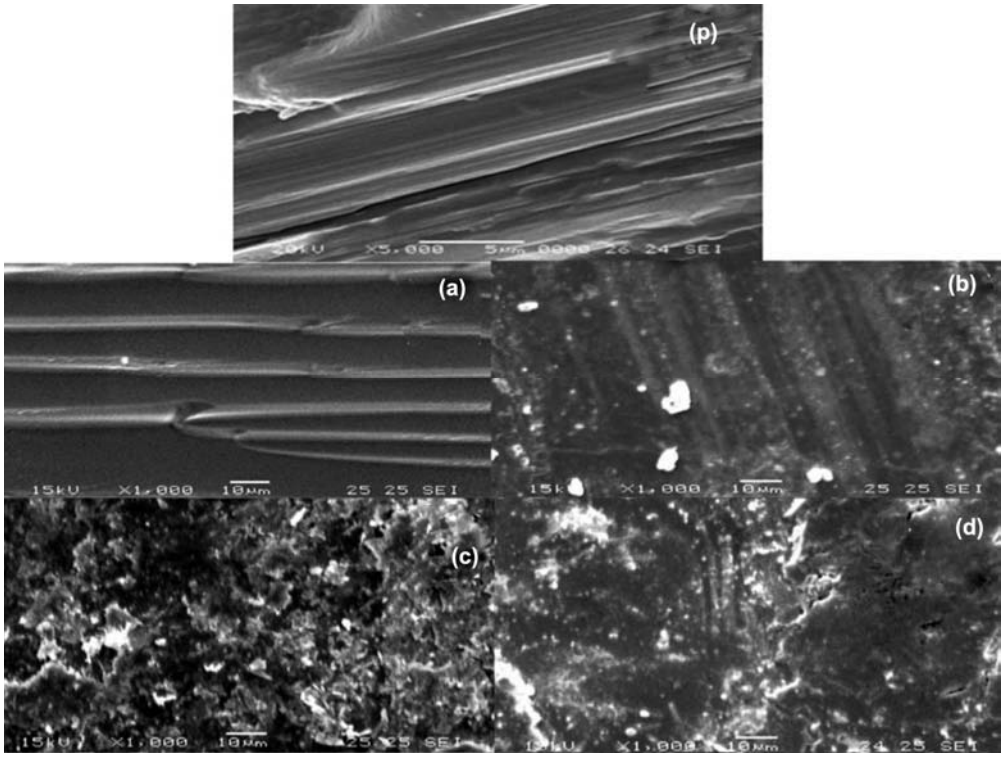

Fig. 2 — SEM micrographs of (p) pure KDP, (a) KDP:Li (b) KDP:Ca (c) KDP:Ce and (d) KDP:V

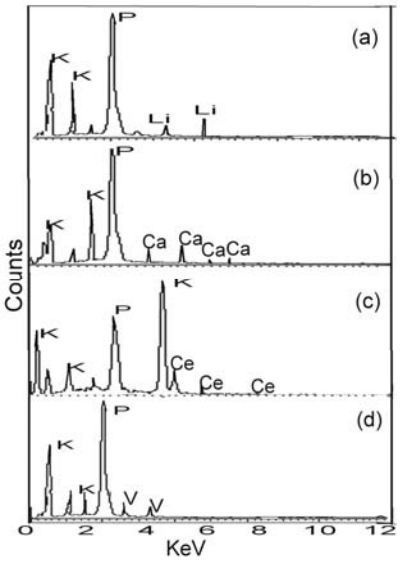

Fig. 3 — EDS spectrum of (a) KDP:Li (b) KDP:Ca (c) KDP:Ce and (d) KDP:V

Table 2 — Amount of metal ion incorporated into the KDP crystalline matrix (by AAS) and direct band-gap energies of doped KDP crystals

Specimen	Quantity of metal ion incorporation (ppm)	Direct band gap energies (eV)
KDP : Li	2.31	5.35
KDP : Ca	2.47	4.95
KDP : Ce	2.11	5.15
KDP : V	1.34	5.05

materials and the thermal patterns are almost similar for all the specimens. The compound is stable and no phase transition is observed. No decomposition up to the melting point ensures the stability of the material for application in laser where the crystals are required to withstand high temperatures. The sharp endotherms are indicative of solid state transition for relatively pure materials (Fig. 5).

The powder XRD patterns of Li(I)-, Ca(II)-, Ce(IV)- and V(V)- doped KDP crystals are compared with that of pure KDP (Fig. 6). The diffraction positions are slightly shifted in the metal doped crystals. The XRD profiles show that all samples were of single phase. General observation is that the relative intensities have been reduced and slight shifts in the peak positions are observed as a result of doping. Extra peaks could be due to the metal dopant. These observations could be attributed to strains in the lattice.

The lattice constants of doped specimens are given in Table 3 and slight changes are observed. It may be

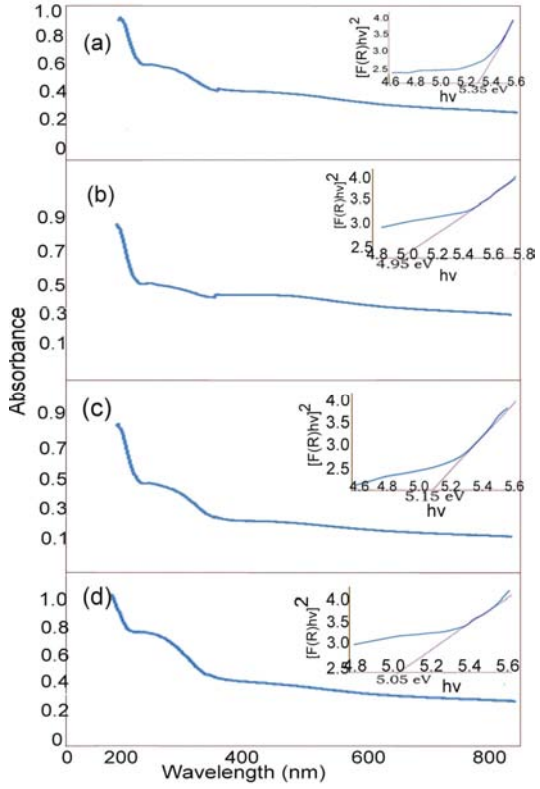

Fig. 4 — UV-Vis spectrum and band-gap energy curves (inner diagram) of (a) KDP:Li (b) KDP:Ca (c) KDP:Ce and (d) KDP:V

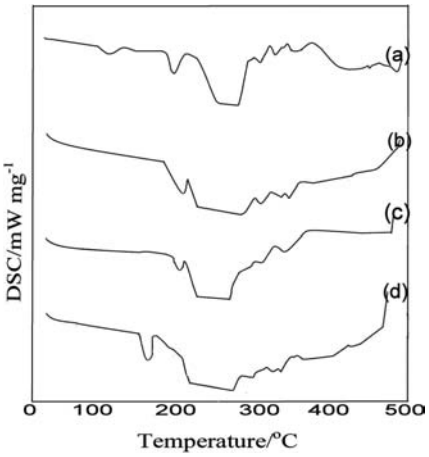

Fig. 5 — DSC curves of (a) KDP:Li (b) KDP:Ca (c) KDP:Ce and (d) KDP:V

mentioned here that the actual concentration of the dopant incorporation in the crystal matrix is small as observed by AAS. The ionic radius of Li(I)-, Ca(II)-, Ce(IV)-and V(V)- are 90, 114, 101 and 68 ppm, respectively[26]. They are very small as compared with that of K^+ (152 pm) and hence, the possibility of dopant incorporation into the KDP crystalline matrix

with minimum distortion and occupation of the substitutional positions is not ruled out. Also, varied valency of dopants can cause a variety of strain related defects.

Figure 7(a) shows the high-resolution diffraction curve (DC) recorded for a typical Li-doped KDP single crystal specimen using (200) diffracting planes in symmetrical Bragg geometry with Mo $K\alpha_1$ radiation. As seen in Fig. 7(a), the DC contains a single peak and indicates that the specimen is free from structural grain boundaries. The full width at half maximum (FWHM) of this curve is 22 arc s which is somewhat more than that expected from the plane wave theory of dynamical X-ray diffraction[27] and reveals the presence of point defects and their aggregates. It is interesting to see the shape of the DC. The DC is asymmetric with respect to the Bragg peak position. The scattered intensity is much more in the positive direction in comparison to that of the negative direction and this feature clearly indicates that the crystal contains predominantly interstitial type of defects than that of vacancy defects. The converse explanation is true in case of vacancy defects which cause tensile stress in the lattice around the defect core leading to increase of lattice spacing and in turn results in more scattered intensity at the lower Bragg angles. It may be mentioned here that the variation in lattice parameter is confined very close to the defect core which gives only the scattered intensity close to the Bragg peak. Long range order could not be expected and hence change in the lattice parameter is also not expected[28]. The defects are more or less statistically distributed in the crystal. If the defects are not statistically distributed but distributed here and there as macroscopic clusters, then the strain generated by such clusters is larger leading to cracks and structural grain boundaries which can be seen very clearly in HRXRD curves with additional peak(s) as observed in our recent study on urea-doped crystals in ZTS at various levels of doping[29]. However, in the present experiments, the diffraction curve does not contain any additional peak and indicates the absence of clustering of point defects at macroscopic level. The single diffraction peak with reasonably low FWHM indicates that the crystalline perfection is quite good.

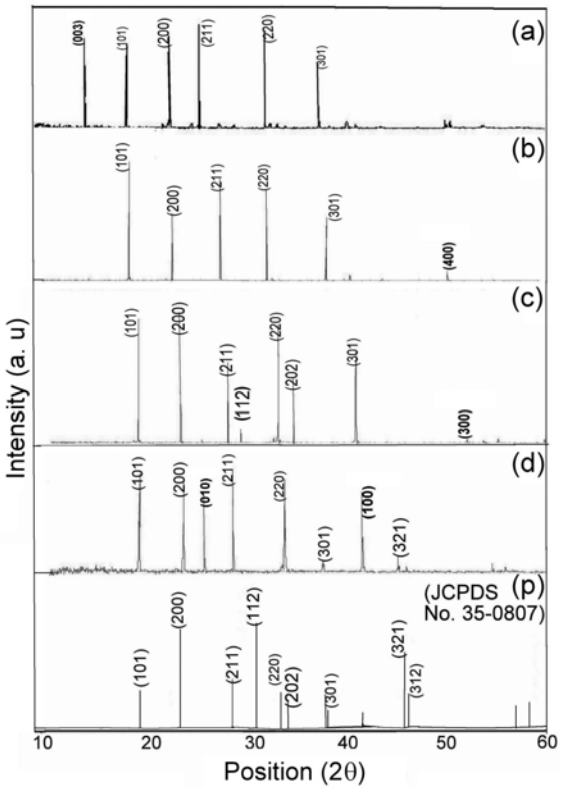

Fig. 6 — Powder XRD spectrum of (a) KDP:Li (b) KDP:Ca (c) KDP:Ce (d) KDP:V and (p) pure KDP

Figure 7(b) shows the DC recorded for a typical Ca-doped KDP single crystal specimen using (200) diffracting planes. It is clear that the curve contains two additional peaks, away from the main peak, depicting internal structural low angle (tilt angle > 1 arc min but less than a deg.) boundaries[30] whose tilt angles (misorientation angle between the two crystalline regions on both sides of the structural grain boundary) are 175 and 232 arc s from their adjoining regions. The FWHM of the main peak and the very low angle boundary are 10, 50 and 166 arc s, respectively. Though the specimen contains low angle

Table 3 — Values of the lattice constants a (Å), b (Å), c (Å) and the cell volume V $(Å)^3$ of 1 mol % metal ion doped KDP crystals

Specimen	*a* (Å)	*b* (Å)	c (Å)	Cell volume $(Å)^3$	System
Pure KDP (JCPDS No. 35-0807)	7.45	7.45	6.97	387	Tetragonal
KDP : Li	7.4620(11)	7.4620(11)	6.9657(11)	386(6)	Tetragonal
KDP : Ca	7.4568(4)	7.4568(4)	6.9678(4)	378(8)	Tetragonal
KDP : Ce	7.4608(8)	7.4608(8)	6.9664(8)	374(4)	Tetragonal
KDP : V	7.4612(4)	7.4612(4)	6.9702(6)	380(6)	Tetragonal

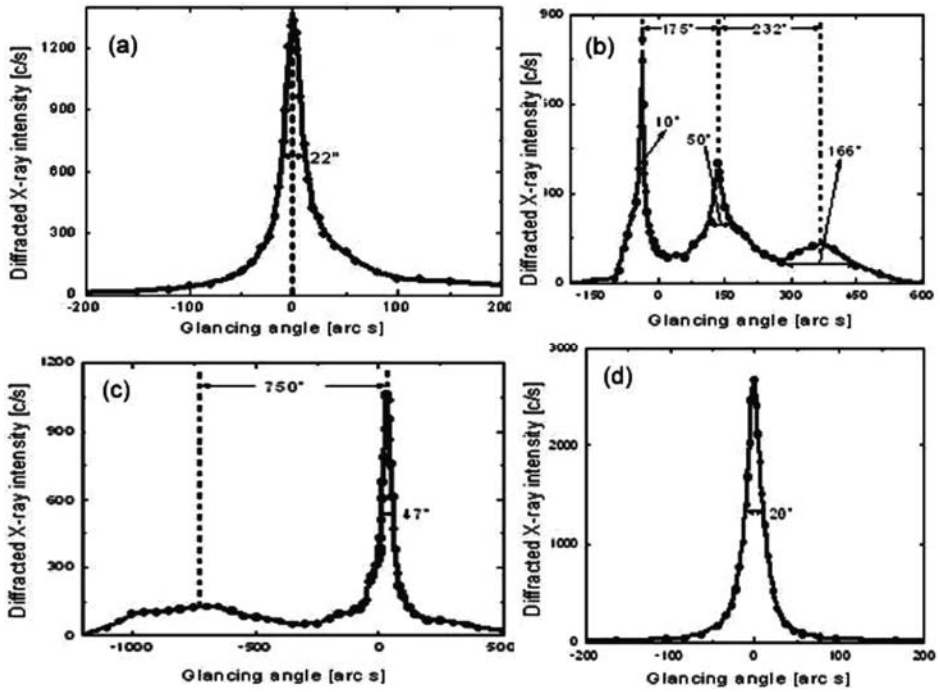

Fig. 7 — High-resolution DCs (a) KDP:Li (b) KDP:Ca (c) KDP:Ce (d) KDP:V

boundaries, the relatively low angular spread of around 600 arc s of the diffraction curve and the low FWHM values show that the crystalline perfection is reasonably good. The strains developed in the crystalline matrix due to incorporation of dopant could be responsible for the observed low angle boundaries.

Figure 7(c) shows the DC recorded for (200) diffraction planes using Mo $K\alpha_1$ radiation for a typical Ce-doped KDP single crystal specimen. From the curve, one can see that in addition to the sharp DC, there is another broad and low intensity peak. The main peak is quite sharp with FWHM of 47 arc s. The additional broad peak depicts a crystalline region in the main crystal with small mosaic blocks which are misorientated to each other by few minutes of arc which might be formed due to release of stress aroused in the crystal from doping. The main sharp peak seems to be due to the denuded crystalline region from excess Ce as observed in excess urea doped ZTS crystals[29].

Figure 7(d) shows the DC recorded for a typical V-doped KDP single crystals using (200) diffracting planes. As seen in Fig. 7(d), the DC contains a single peak and indicates that the grown crystal is free from structural grain boundaries. The FWHM (full width at half maximum) value of the curve is 20 arc s. This value is quite higher than that expected from the plane wave theory of dynamical X-ray diffraction[27]. This broadening of rocking curve without the presence of any splitting and without much asymmetry with respect to the peak position can be attributed to the presence of vacancy defects as well as interstitially incorporated dopants in the crystalline matrix[31]. When the density of such defects is lesser or moderate and when the size of the dopants is not high as in the present case, they can accommodate inside the crystalline matrix and they hardly develop any strain. If the strain is high, the FWHM would be much higher and often lead to structural grain boundaries[32]. Point defects up to some extent are unavoidable due to thermodynamical considerations and growth conditions[33]. The observed scattering due to point defects is of short range order as the strain due to such minute defects is limited to the very defect core and the long range order could not be expected which may lead to change in the lattice parameter.

The intensity of SHG outputs gives an indication of the non-linear optical character of the material. The doubling of frequency is confirmed by green radiation at 532 nm. The efficient SHG demands specific molecular alignment of crystals to be achieved facilitating non-linearity in the presence of dopant. SHG outputs are listed in Table 4. Li(I)-, Ca(II)-, Ce(IV)- and V(V)- doping significantly improves the SHG efficiency because of facile charge transfer.

Table 4 — SHG outputs

Specimen	$I_{2\omega}$ (mV)
Pure KDP	34
KDP : Li	48
KDP : Ca	47
KDP : Ce	42
KDP : V	45

Interesting to observe that irrespective of the nature of metal and varied ionic charges, doped metal tunes the electronic properties of host metal and improves the SHG efficiency.

4 Conclusions

A comparative study is made for the effect of impurities with varied ionic charges ranging from +1 to +5 on KDP. We have used XRD, FT-IR, SEM, EDS, AAS, UV-Vis, DSC, HRXRD and Kurtz powder technique to investigate the influence of cations Li(I)-, Ca(II)-, Ce(IV)- and V(V)- doping on KDP crystals. Interesting to observe that the incorporation of metal dopant even at low doping levels are well established by AAS and EDS techniques. The reduction in the intensities observed in XRD and slight shifts in vibrational frequencies in FT-IR reveal minor structural variations in the KDP crystalline matrix by doping. DSC studies reveal the purity of the material and no decomposition is observed up to the melting point. UV-Vis spectrum shows that the transparency of the crystal has not been affected significantly by the metal ion dopant. Varied surface morphologies as a result of doping ions are observed by SEM micrographs. Irrespective to the nature of the metal and ionic charge enhanced efficiency is, generally, observed with metal doping.

References

1 Zaitseva N & Carman L, *Prog Cryst Growth Charact,* 43 (2001)1.
2 Klimentov S M, Garnov S V, Epifanov A S & Manenkov A A, *Prog SPIE,* 2145 (1994) 342.
3 R Ramirez & Gonzala J A, *Solid State Commun,* 75 (1990) 482.
4 West J, *Z Kristallogr*, 74 (1930) 306.
5 Belout G, Dunia E & Petroff J F, *J Cryst Growth*, 23 (1974) 243.
6 Rashkovich L N & Kronsky N V, *J Cryst Growth*, 182 (1997) 434.
7 Thomas T N, Land T A, Johnson M & Casey W H, *J Coll Interf Sci,* 280 (2004) 18.
8 Kannan V, Ganesh R Bairava, Satyalakshimi R, Rajesh N P & Ramasamy P, *Cryst Res Technol,* 41 (2006) 678.
9 Ioanid A, *J Optoelectonic Advance Mater,* 2(2000) 275.
10 Kumari R Ananda & Chandramani R, *Bull Mater Sci,* 26 (2003) 255.
11 Jayaprakasan M, Rajesh N P, Kannan V, Ganesh R Bairava, Bhagavannarayana G & Ramasamy P, *Mater Lett,* 61 (2007) 2419.
12 Voronov A P, Babenko G N, Puzikov V M, Roshal A D & Salo V I, *Crystallography Reports,* 53 (2008) 708.
13 Salo V I, Tkachenko V F, Voronov A P, Puzikov V M & Tsurikov V A, *Functional Mater,* 12 (2005) 658.
14 Lai X, Roberts K J, Bedzyk M J, Lyman P F, Cardoso L P & Sasaki J M, *Chem Mater,* 17 (2005) 4053.
15 Rak M, Eremin N N, Eremina E A, Kuznetsov V A, Okhrimenko T M, Furmanova N G & Efremova E P, *J Cryst Growth,* 273 (2005) 577.
16 Eremina T A, Kuznetsov V A, Eremin N N, Okhrimenko T M, Furmanova N G, Efremova E P & Rak M, *J Cryst Growth*, 273 (2005) 586.
17 Fu Y J, Gao Z S, Sun X, Wang S L, Li Y P, Zeng H, Luo J P, Duan A D & Wang J Y, *Cryst Growth & Charact,* 2000, 40, 211.
18 Fu Y J, Gao Z S, J M Liu, Li Y P, Zeng H & Jiang M H, *J Cryst Growth,* 198 (1999) 682.
19 Ramasamy G, Bhagavannarayana G & Meenakshisundaram S, *Cryst Eng Comm,* 14 (2012) 3813.
20 Lal K & Bhagavannarayana G, *J Appl Cryst,* 22 (1989) 209.
21 Bhagavannarayana G & Kushwaha S K*, J Appl Cryst,* 43 (2010) 154.
22 Bhagavannarayana G, Parthiban S & Meenakshisundaram Subbiah, *J Appl Cryst,* 39(2006) 784.
23 Kulbelka P, *J Opt Soc Am,* 38 (1948) 448.
24 Lin Z, Wang Z, Chen C & Lee M H, *J Chem Phys,* 118 (2003) 2349.
25 Dimitriev V G, Gurzaddyan G G & Nikogosyan D N, *Handbook of Nonlinear Optical Crystals*, 2nd revised Edison., Springer, Berlin, (1977).
26 Huheey J E, Keiter E A & Keiter R L, Inorganic Chemistry principles of structure & reactivity, Pearson Education Asia, Fourth edition, (2002) 112.
27 Batterman B W & Cole H, *Rev Mod Phys,* 36 (1964) 681.
28 Bhagavannarayana G, Kushwaha S K, Shakir Mohd & Maurya K K, *J Appl Cryst,* 44 (2010) 122.
29 Bhagavannarayana G & Kushwaha S K, *J Appl Cryst,* 43 (2010) 154.
30 Bhagavannarayana G, Ananthamurthy R V, Budakoti G C, Kumar B & Bartwal K S, *J Appl Cryst,* 38 (2005) 768.
31 Senthilkumar K, MoorthyBabu S & Bhagavannarayana G, *J Appl Cryst,* 44 (2011) 313.
32 Bhagavannarayana G, Parthiban S & Meenakshisundaram Subbiah, *Crystal Growth & Design,* 8 (2008) 446.
33 Bhagavannarayana G, Rajesh P & Ramasamy P, *J Appl Cryst,* 43 (2010) 1372.